

Cite this: *Dalton Trans.*, 2021, **50**, 9540

## Crystal transformation in Mn(II) metal–organic frameworks based on a one-dimensional chain precursor†

Yansong Jiang,  Rui Liu, Yiran Gong, Yong Fan,  Li Wang \* and Jianing Xu\*

The solvothermal reaction of Mn(II) salts and 5-((4'-(tetrazol-5'-yl)benzyl)oxy)isophthalic acid ( $H_3L$ ) affords an Mn(II) based coordination polymer  $Mn(H_2L)_2(H_2O)_2$  (**1**), which possesses a one-dimensional (1D) chain structure. Using **1** as the precursor, three Mn(II) metal–organic frameworks,  $Mn_3L_2(2,2'-bpy)_2 \cdot 5H_2O$  (**2**),  $Mn_3L_2(H_2O)_4$  (**3**), and  $Mn_4L_2(HL)(H_2O)_5 \cdot 0.5H_2O$  (**4**), with three-dimensional (3D) networks can be obtained by different strategies of crystal transformation. Upon introduction of 2,2'-bipyridine (2,2'-bpy) as the ligand and 2,2'-biquinoline-4,4'-dicarboxylic acid as the structural-directing agent, **1** undergoes irreversible crystal transformation into **2** and **3**, respectively, and **1** can be transformed into **4** by increasing the reaction temperature. Interestingly, the irreversible structural transformation of **3** into **2** can be carried out by adding a 2,2'-bpy ligand. Notably, after the removal of coordinated water molecules, **1** and **3** exhibit good catalytic performance for the cyanosilylation reaction even at 0 °C.

Received 23rd March 2021,  
Accepted 28th May 2021

DOI: 10.1039/d1dt00943e

rsc.li/dalton

## Introduction

Over the last two decades, as a class of well-defined inorganic–organic hybrid crystalline materials, metal–organic frameworks (MOFs) have attracted more attention due to their versatile structures and wide applications in gas adsorption and separation, chemical sensing, catalysis, energy storage, and medicine.<sup>1–10</sup> Although many MOFs with interesting topologies have been reported by tuning their metal centers, the types of organic ligands, counter-ions, metal-to-ligand ratios or solvent systems, the control of the framework dimensionality and properties of MOFs is still a huge challenge.<sup>11–13</sup>

Single-crystal transformation is a fantastic approach to construct versatile MOFs with changes in dimensionality and properties such as luminescence, magnetism, and catalysis.<sup>14–16</sup> Generally, crystal transformation should break the original coordination bonds and force the formation of new stable coordination bonds, which can strengthen the framework stability.<sup>17</sup> To date, crystal transformation of MOFs can be achieved by exchange of metal centers and introduction of

additional ligands as well as external stimuli such as temperature, solvents, or vapors.<sup>17,18</sup> Using a low-dimensional crystal as a precursor, especially an insoluble precursor, is one of the effective strategies to alter the structures and properties of MOFs and to incorporate functionalities of interest.<sup>19</sup> For example, Jiang *et al.* reported a series of single-crystals of  $[Ti_8Zr_2O_{12}(COO)_{16}]$  clusters based on several small acid ligand molecules, and these clusters could be used as the precursor in the synthesis of single crystals of PCN-415 (PCN = porous coordination network) by introducing the additional terephthalic acid ligand.<sup>20</sup> Park *et al.* reported a Ti-MOF derived from a 0D Ti-oxo cluster precursor which was used to prepare DGIST-1 with a 3D network by adding a porphyrinic ligand.<sup>21</sup>  $[Mn_4(H_2O)_{18}WZnMn_2(H_2O)_2(ZnW_9O_{34})_2]^{4-}$ , a 1D anionic chain precursor, can transform into two 3D solid frameworks upon introduction of additional transition metal ions and solvent molecules.<sup>22</sup>

In this work, we selected a flexible N-heterocyclic carboxylate ligand, 5-((4'-(tetrazol-5'-yl)benzyl)oxy)isophthalic acid ( $H_3L$ ), to react with Mn(II) salts for preparing new Mn(II) based metal–organic frameworks with interesting catalytic performance. Firstly,  $Mn(H_2L)_2(H_2O)_2$  (**1**) with a one-dimensional (1D) chain structure was successfully prepared by the self-assembly of Mn(II) salts and  $H_3L$  under solvothermal conditions. Then using **1** as the precursor, three Mn(II) MOFs,  $Mn_3L_2(2,2'-bpy)_2 \cdot 5H_2O$  (**2**),  $Mn_3L_2(H_2O)_4$  (**3**), and  $Mn_4L_2(HL)(H_2O)_5 \cdot 0.5H_2O$  (**4**), with three-dimensional (3D) networks were obtained through different routes of crystal transformation. Upon introduction of 2,2'-bipyridine (2,2'-bpy) as the ligand and 2,2'-biquinoline-

State Key Laboratory of Inorganic Synthesis & Preparative Chemistry,  
College of Chemistry, Jilin University, Changchun, 130012 Jilin Province, P. R. China.  
E-mail: hwang99@jlu.edu.cn, xujn@jlu.edu.cn

† Electronic supplementary information (ESI) available: Simplified structures, PXRD patterns, FT-IR spectra, TG curves,  $N_2$  adsorption data, crystal data and structure refinement details, selected bond lengths and angles and H-bond information. CCDC 2062075–2062077. For ESI and crystallographic data in CIF or other electronic format, see DOI: 10.1039/d1dt00943e

4,4'-dicarboxylic acid as the structural-directing agent, **1** undergoes irreversible crystal transformation into **2** and **3** respectively, and **1** can be transformed into **4** by increasing the reaction temperature. Furthermore, **3** can be transformed into **2** by adding a 2,2'-bpy ligand and into **4** by prolonging the reaction time. In addition to the intriguing structures, the activated **1-3** can be used as heterogeneous catalysts for the cyanosilylation of different aldehydes under solvent-free conditions at room temperature and 0 °C. The diverse structures and different catalytic active sites of **1-3** result in distinct catalytic activities.

## Experimental

### Synthesis of **1-4**

**Mn(H<sub>2</sub>L)<sub>2</sub>(H<sub>2</sub>O)<sub>2</sub> (1).** MnCl<sub>2</sub>·4H<sub>2</sub>O (0.0197 g, 0.10 mmol), H<sub>3</sub>L (0.0240 g, 0.07 mmol), acetonitrile (4 mL) and deionized water (3 mL) were added into a 25 mL Teflon-lined vessel and sealed in an autoclaved reactor for 2 days at 120 °C. After cooling to room temperature, colorless crystals were obtained. The yield was 63% (0.0522 g) based on Mn. Calcd for **1**: C, 46.60; H, 3.15; N, 13.59. Found: C, 46.35; H, 3.19; N, 13.34. FT-IR (KBr, cm<sup>-1</sup>): 3220(m), 1690(s), 1596(s), 1440(m), 1374(m), 1270(m), 1237(m), 1199(s), 1147(m), 1057(s), 1019(w), 958(w), 882(w), 821(m), 765(m), 685(w), 580(w), 491(w).

**Mn<sub>3</sub>L<sub>2</sub>(2,2'-bpy)<sub>2</sub>·5H<sub>2</sub>O (2).** 2,2'-Bpy (0.0100 g, 0.64 mmol) was placed in a reactor filled with single-crystals of **1** (10 mg), acetonitrile (4 mL) and deionized water (3 mL) and sealed in an autoclaved reactor for 2 days at 140 °C. After cooling to room temperature, light yellow crystals were collected. The yield was 83% (8.3 mg) based on **1**. Calcd for **2**: C, 40.49; H, 2.86; N, 10.90. Found: C, 40.05; H, 3.72; N, 11.07. FT-IR (KBr, cm<sup>-1</sup>): 3394(s), 3083(w), 2861(w), 1605(m), 1553(s), 1449(s), 1383(s), 1322(w), 1265(m), 1132(w), 1048(m), 1010(m), 935(w), 859(w), 830(w), 770(m), 717(m), 646(w), 580(w), 562(w), 452(w), 424(w).

**Mn<sub>3</sub>L<sub>2</sub>(H<sub>2</sub>O)<sub>4</sub> (3).** 2,2'-Biquinoline-4,4'-dicarboxylic acid (H<sub>2</sub>bqdc) (0.0100 g, 0.31 mmol) was placed in a reactor filled with single-crystals of **1** (10 mg), acetonitrile (4 mL) and deionized water (3 mL) and sealed in an autoclaved reactor for 2 days at 160 °C. After cooling to room temperature, light yellow crystals were collected. The yield was 72% (7.2 mg) based on **1**. Calcd for **3**: C, 42.15; H, 3.07; N, 12.29. Found: C, 42.05; H, 3.22; N, 12.43. FT-IR (KBr, cm<sup>-1</sup>): 3450(s), 1614(w), 1580(s), 1518(s), 1446(s), 1413(m), 1384(s), 1361(s), 1308(w), 1265(w), 1146(w), 1041(w), 997(w), 806(w), 773(s), 710(m), 663(w), 634(w), 486(w), 428(w).

**Mn<sub>4</sub>L<sub>2</sub>(HL)(H<sub>2</sub>O)<sub>5</sub>·0.5H<sub>2</sub>O (4).** Single-crystals of **1** (10 mg), acetonitrile (4 mL) and deionized water (3 mL) were placed in an oven for 2 days at 140 °C. Single-crystals of **4** were prepared according to the reported procedure.<sup>23</sup>

### Catalytic experiment

The crystalline samples were immersed in CHCl<sub>3</sub> for one day and heated at 120 °C under vacuum overnight for activation.<sup>24-26</sup>

For cyanosilylation, the activated **1-3**, trimethylcyanosilane (TMSCN, 2 mmol), and aldehydes (1 mmol) were added into a 4 mL reactor and stirred at room temperature. The reactions were monitored by <sup>1</sup>H NMR spectroscopy and the yield was calculated based on the sum of the integral of product/(product + aldehydic substrates).<sup>27</sup>

The recycling studies were performed under the same conditions as mentioned previously, except for using the recycled catalysts in the last run. After each run of the reaction, the solid-state catalyst was separated from the mixture by centrifugation and washed three times with CHCl<sub>3</sub>, and the recycled catalyst was dried at 80 °C for the next run.

## Results and discussion

### Crystal structure description

Single-crystal X-ray diffraction studies revealed that **1** crystallizes in the triclinic system, *P* $\bar{1}$  space group, and the asymmetric unit contains one crystallographically independent Mn atom. As shown in Fig. 1a, Mn1 is coordinated with two carboxylate oxygen atoms and two nitrogen atoms from two individual H<sub>2</sub>L<sup>-</sup> ligands, and the other two oxygen atoms are from the coordinated water molecules, forming a slightly distorted MnO<sub>4</sub>N<sub>2</sub> octahedron. The Mn–O bond lengths and Mn–N bond lengths are in good agreement with the ranges reported for Mn-based MOFs.<sup>28-32</sup> Interestingly, eight Mn atoms are located in the eight vertexes of the unit cell and each Mn atom occupied 1/8th in one unit cell. The carboxylate groups of the organic ligand are protonated. Each H<sub>2</sub>L<sup>-</sup> ligand links two Mn (II) cations through one monodentate carboxylate group and one tetrazole nitrogen atom. As shown in Fig. 1b, two H<sub>2</sub>L<sup>-</sup> ligands link two MnO<sub>4</sub>N<sub>2</sub> polyhedra forming the infinite one-dimensional rectangle ring chain along the *b* axis. The free-carboxylate groups decorate the infinite chain and point to the outside of the chain. The distance between a tetrazole ring and a benzene ring is 3.86(3) Å and the distance between two benzene rings is 3.88(5) Å, indicating that there are continuous weak  $\pi$ - $\pi$  interactions in the structure of **1** (Fig. 1c). Extensive hydrogen bonds also exist among the coordinated water mole-

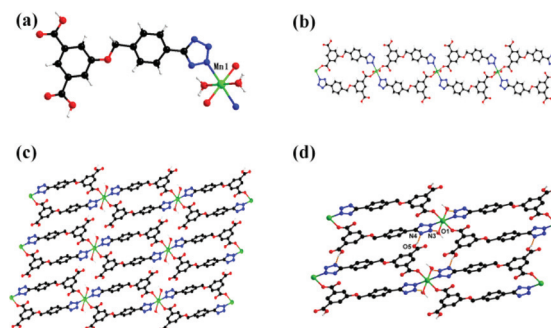


**Fig. 1** (a) The coordination environment of the Mn center in **1**. (b) The one-dimensional chain in **1**. (c) The stacking fashion in the *ac* plane. (d) The hydrogen-bond interactions in **1**.

cules, carboxylate groups and tetrazole units. The coordinated water molecules and the free-carboxylate group form two strong hydrogen bonds with the nitrogen atoms from the tetrazole rings of another chain ( $d_{O1...N3} = 2.81(2)$  Å;  $d_{O5...N4} = 2.70(4)$  Å) (Fig. 1d). Because of the H-bond interactions and continuous  $\pi$ - $\pi$  interactions, the infinite chains of **1** construct a 3D supramolecular structure.

**2** crystallizes in the monoclinic system,  $C2/c$  space group. As illustrated in Fig. 2a, there are two independent Mn atoms in the asymmetric unit. Both Mn atoms adopt a six-coordinated mode, and Mn1 is coordinated with four carboxylate oxygen atoms from four individual  $L^{3-}$  ligands and two tetrazole nitrogen atoms, while Mn2 is coordinated with three carboxylate oxygen atoms from two individual  $L^{3-}$  ligands, one tetrazole nitrogen atom and two other nitrogen atoms from the 2,2'-bpy unit. The carboxylate groups in the ligand are completely deprotonated. It is noted that one  $L^{3-}$  ligand links six Mn(II) cations by its two carboxylate groups and one tetrazole motif in a  $(\kappa^1-\kappa^1-\mu_2)-(\kappa^2-\kappa^1-\mu_3)-(\kappa^1-\kappa^1-\mu_2)-\mu_7$  coordination fashion. The 2,2'-bpy is coordinated with one Mn(II) cation in a classic chelating fashion. One Mn1 and two Mn2 atoms form a trinuclear  $Mn_3O_8N_8$  unit, in which the Mn1 atom locates in the center and connects with the other two Mn2 atoms by vertex-sharing mode (Fig. 2b). Each trinuclear unit links six  $L^{3-}$  ligands and extends to a three-dimensional framework (Fig. 2c). From the topology point of view, the trinuclear unit can be regarded as a six-connected node and the  $L^{3-}$  ligand can be seen as a three-connected node (Fig. S2†). Thus, the framework of **2** can be simplified as a 3,6-connected network with a Schläfli symbol of  $\{4^2 \cdot 6\}_2\{4^4 \cdot 6^2 \cdot 8^8 \cdot 10\}$  (Fig. 2d).

**3** crystallizes in the monoclinic system,  $P2_1/c$  space group. As shown in Fig. 3a, there are two crystallography independent Mn atoms and one  $L^{3-}$  ligand. The two Mn atoms are both in a six-coordinated fashion and adopt a slightly distorted octahedral coordination geometry. Mn1 coordinates with four carboxylate oxygen atoms from  $L^{3-}$  and the other two are nitrogen atoms from the tetrazole unit, and Mn2 coordinates with three carboxylate atoms, two coordinated water molecules and one

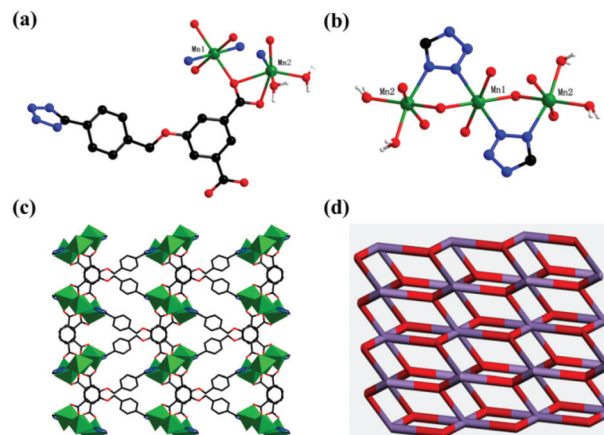


Fig. 3 (a) The coordination environment of the Mn centers in **3**. (b) The  $Mn_3O_{12}N_4$  unit. (c) The 3D view of **3** in the  $ab$  plane. (d) The schematic representation of the topology for **3**.

tetrazole nitrogen atom. Moreover, the  $L^{3-}$  ligand links six Mn(II) cations by its two carboxylate groups and one tetrazole moiety in the  $(\kappa^1-\kappa^1-\mu_2)-(\kappa^2-\kappa^1-\mu_3)-(\kappa^1-\kappa^1-\mu_2)-\mu_7$  coordination fashion. One Mn1 and two Mn2 atoms are connected with each other forming a  $Mn_3O_{12}N_4$  trinuclear unit, where the Mn1 atom is located in the center and connects with two Mn2 atoms *via* sharing vertex oxygen atoms (Fig. 3b). The  $L^{3-}$  ligands connect with adjacent trinuclear units to accomplish a three-dimensional framework. It is noted that the organic ligand in the structure of **3** is disordered, and the ADPs image is illustrated in Fig. S3a.† Topologically, the trinuclear unit can be viewed as a six-connected node and  $L^{3-}$  is regarded as a three-connected node (Fig. S3b†). Consequently, the framework of **3** can be simplified as a 3,6-connected network with a Schläfli symbol of  $\{4 \cdot 6^2\}_2\{4^2 \cdot 6^{10} \cdot 8^3\}$  (Fig. 3d).

According to our previous work, the two coordination modes of the  $H_3L$  ligand mentioned above are two new coordination modes, noted as **IV** and **V** (Fig. 4). Owing to the rotation of the ether oxygen atom and the  $-CH_2-$  group, the flexible  $H_3L$  ligand has variable coordination modes. As shown in Fig. S4,† the angles between the benzene ring planes are  $13.73^\circ$  for **IV**,  $57.51^\circ$  for **V-1**, and  $28.69^\circ$  for **V-2** while those for **I-III** are  $23.61^\circ$ ,  $40.10^\circ$ , and  $20.93^\circ$ , respectively. Notably, despite the fact that the coordination modes of  $L^{3-}$  in **2** and **3**

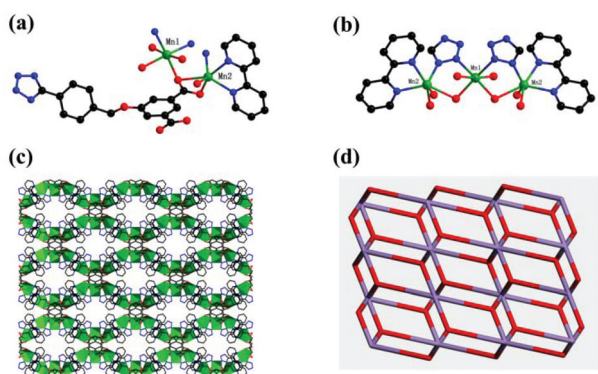


Fig. 2 (a) The coordination environment of the Mn centers in **2**. (b) The  $Mn_3O_8N_8$  unit. (c) The 3D view of **2** in the  $ab$  plane. (d) The schematic representation of the topology for **2**.

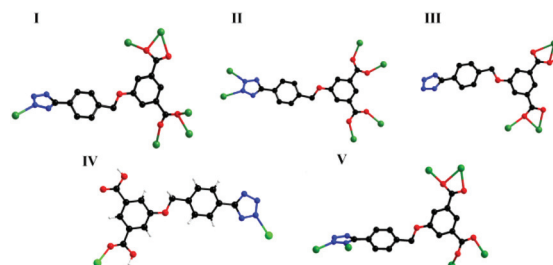


Fig. 4 The coordination modes of the organic ligand.

are both **V**, their conformations are different due to the flexibility of the  $L^{3-}$  ligand. The angles between the benzene ring planes in **2** and **3** are  $57.51^\circ$  and  $28.69^\circ$ , respectively, and the angles between a benzene ring and a tetrazole ring are  $31.75^\circ$  and  $49.98^\circ$ , respectively. Therefore, the conformational isomerism of the  $L^{3-}$  ligand may directly lead to the difference in structures of **2** and **3**.

### Crystal transformation

First, colorless rhomboid block crystals of **1** were synthesized through the solvothermal reactions of  $Mn(II)$  salts and  $H_3L$ . Then, single-crystals of **1** and the solvent were heated at  $140^\circ C$  for another 2 days (Fig. 5). Subsequently, light yellow rod single-crystals of **4** were obtained, and the purity of the product was proved by PXRD analysis, indicating that **1** completely transformed into **4**. Moreover, 10 mg of 2,2'-bpy as an additional ligand was added to **1** and the solvent. Afterward, light yellow cubic single-crystals of **2** were acquired under solvothermal conditions. The purity of the final product was also confirmed using the PXRD pattern (Fig. S6†). Encouraged by the successful transition of **1** to **2**, we used  $H_2bqdc$  as the alternative of 2,2'-bpy to synthesize the coordination network. Notably,  $H_2bqdc$  did not coordinate to the backbone of the final structure but acted as a structural-directing agent inducing new coordination networks. Moreover, **1** could not transform into a pure product of **3** but a mixture of **3** and **4** by crystal transformation (Fig. S7†). The pure product of **3** could be achieved by a one-pot synthesis method (Fig. S8†). In addition, due to the similar building units and topological networks of **2** and **3**, the transformation of **3** into **2** was also investigated. 10 mg of 2,2'-bpy was added to single-crystals of **3** and their mother solution and heated for 2 days at  $140^\circ C$ .

As a result, single-crystals of **2** could be achieved which suggested that the coordinated water molecules in **3** were replaced by the 2,2'-bpy ligand and resulted in the structural transformation. Meanwhile, single-crystals of **3** can be partially converted into **4** by prolonging the reaction time (Fig. S10†). Unfortunately, even if the reaction time is extended to seven

days, the product is still a mixture of **3** and **4**. Thus, **3** cannot be completely converted into **4** by prolonging the reaction time. This transformation from **1** to **2–4** may be caused by rearrangement or dissociation to its constituent parts under the pressure and temperature conditions. These results demonstrated that **2** and **4** may be thermodynamically very stable compounds because **2** or **4** could not transform into other compounds. Meanwhile, **1** may be an intermediate state in the syntheses of **2–4**. Thus, external stimuli including additional ligand, structural-directing agent and temperature played important roles in the construction of  $Mn(II)$ -MOFs based on the  $H_3L$  ligand.

### Characterization

The PXRD patterns of **1–3** matched well with the simulated ones calculated using single-crystal X-ray diffraction data, indicating that the as-synthesized samples of **1–3** are the pure phase. The differences between the simulated patterns and as-synthesized patterns are due to the different crystal orientations of the powder samples.

The thermogravimetric analyses of **1–3** were performed under an air atmosphere (Fig. S12†). For **1**, there are two obvious weight loss steps. The first step from  $113$  to  $206^\circ C$  is due to the loss of coordinated water molecules (calculated: 4.37%, found: 4.39%). The second step of weight loss from  $152$  to  $492^\circ C$  can be due to the decomposition of the framework. For **2**, the first step of weight loss before  $315^\circ C$  corresponds to the loss of five free water molecules (calculated: 5.84%, found: 5.60%), and the second weight loss from  $315$  to  $537^\circ C$  is due to the decomposition of the framework. For **3**, the first step of weight loss before  $300^\circ C$  is due to the loss of four coordination water molecules (calculated: 7.99%, found: 7.81%). The second step of weight loss from  $300$  to  $458^\circ C$  can be ascribed to the collapse of the framework (calculated: 26.02%, found: 27.27%). The final products of these three MOFs after TGA are  $\alpha-Mn_2O_3$  (PDF#41-1442) which can be verified by PXRD analysis (Fig. S13†).

The porosity of these MOFs has been characterized using  $N_2$  adsorption isotherms at  $77\text{ K}$ . As shown in Fig. S14,† **3** exhibited a type I adsorption curve and the BET surface area is  $162\text{ m}^2\text{ g}^{-1}$  and the pore width is about  $1.18\text{ nm}$  which agrees with the single-crystal XRD data; however, **1** and **2** showed no obvious  $N_2$  uptake.

### Catalytic properties

As we all know, after removing the coordinated solvent molecules, unsaturated coordinated metal centers can be viewed as Lewis acid sites for heterogeneous catalysis.<sup>33–36</sup> The cyanosilylation of aldehyde is a typical acid-catalyzed condensation reaction and is widely used as a reaction to detect Lewis acidity in MOFs.<sup>37,38</sup> Thus, after activation, **1–3** were used for cyanosilylation of aldehyde to study their catalytic performances. As illustrated in Table 1, when the solvent was  $CDCl_3$ , the yields were 86%, 52%, and 61%, and the yields were 90%, 50% and 72% under solvent-free conditions (entries 1 and 2). Thus, to achieve a higher catalytic efficiency at low cost, the catalysis

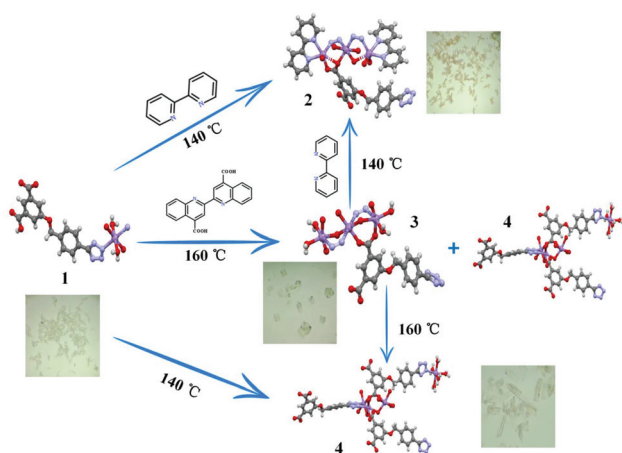


Fig. 5 Schematic illustration of crystal transformations between **1–4**.

Table 1 The cyanosilylation reactions catalyzed by 1–3<sup>a</sup>

Entry	Substrate	Temperature	Solvent	Yield (%)		
				1	2	3
1	Benzaldehyde	r.t.	CDCl <sub>3</sub>	86	52	61
2	Benzaldehyde	r.t.	Solvent-free	90	50	72
3	<i>o</i> -Fluorobenzaldehyde	r.t.	Solvent-free	>99	15	99
4	<i>o</i> -Bromobenzaldehyde	r.t.	Solvent-free	>99	38	70
5	<i>o</i> -Methoxybenzaldehyde	r.t.	Solvent-free	80	50	71
6	<i>o</i> -Cyanobenzaldehyde	r.t.	Solvent-free	>99	99	>99
7	<i>p</i> -Cyanobenzaldehyde	r.t.	Solvent-free	>99	>99	>99
8	<i>m</i> -Cyanobenzaldehyde	r.t.	Solvent-free	95	65	74
9	1-Naphthaldehyde	r.t.	Solvent-free	54	49	52
10	9-Anthraldehyde	r.t.	Solvent-free	50	48	50
11	Pyridine-4-carboxaldehyde	r.t.	Solvent-free	99	99	99
12	1-Phenylethanone	r.t.	Solvent-free	>99	>99	>99
13	Acetaldehyde	r.t.	Solvent-free	>99	68	99
14	Propionaldehyde	r.t.	Solvent-free	>99	51	90
15	Valeraldehyde	r.t.	Solvent-free	99	27	59
16	Cinnamaldehyde	r.t.	Solvent-free	54	37	84
17	Benzaldehyde	0 °C	Solvent-free	74	—	62

<sup>a</sup> Reaction conditions: TMSCN (2 mmol), aldehydes (1 mmol), catalyst (0.5 mol%), solvent. r.t.: room temperature.

experiments were performed under solvent-free conditions. In order to explore the applicability of these three catalysts to different substrates, the reactions between aldehydes with different substitute groups and TMSCN under the same conditions were carried out. When the substitute group is *o*-F and *o*-Br, the yields of the product are >99% and >99% for 1, 15% and 38% for 2, and >99% and 70% for 3. With the electron-donating group *o*-OCH<sub>3</sub>, the yields were 80%, 50% and 71%; when the electron-withdrawing group *o*-CN was applied, both the yields were over 99%. Thus, the electronic effects of the substitute groups have an obvious influence on the reaction. The position of the substitute group also has an impact on this reaction. The yields of *o*-CN and *p*-CN groups were over 99%; however, those of *m*-CN were decreased to 95%, 65%, and 74%, respectively. Moreover, the larger size substrate has a low yield (entries 6–8). As for pyridine-4-carboxaldehyde, 1-phenylacetaldehyde, acetaldehyde, propionaldehyde and valeraldehyde, high yield can be obtained, which indicated that activated 1–3 have good catalytic activity for the heterocyclic and aliphatic aldehydes. When cinnamaldehyde was used as the substrate, the yield decreased to 64%, 37%, and 84%, respectively. Furthermore, in order to broaden the range of use of the catalyst, the catalytic experiment was performed at 0 °C. The yields of 1 and 3 were 60% and 57% after 3 h, and 74% and 62% after 6 h. It is noted that the catalytic performances for 1 and 3 are much higher than that for 2. The reason is that there are no coordinated solvent molecules in the structure of 2, and at the same time, the Mn center is six-coordinated and almost no Lewis acidity is observed in the metal

center, while the Mn center in the structure of 1 and 3 is coordinated with two water molecules which can be removed by activation and then displays Lewis acidic sites. In addition, there is no Lewis acidic site in 2, but the catalytic property probably originated from the basic catalytic sites in the ligand.<sup>39,40</sup> Additionally, MnCl<sub>2</sub>·4H<sub>2</sub>O, H<sub>3</sub>L and a physical mixture of MnCl<sub>2</sub>·4H<sub>2</sub>O and H<sub>3</sub>L are also employed as homogeneous catalysts for the cyanosilylation of aldehyde. Their yields can reach 99%; however, they are too difficult to separate from the reaction system to reuse.

In order to prove the heterogeneous feature of the catalysts, the solid-state catalysts were removed from the reaction system by centrifugation after 0.5 h. The reaction process shuts down quickly after removing the catalyst. Even if the reaction system standing for another 1 h, the yield is not increase anymore which indicates that no homogeneous species is present in the reaction system (Fig. 6a). The recyclability of the heterogeneous catalysts is an important feature for the application. Thus, the catalysts of 1–3 were separated after catalysis, washed three times with CHCl<sub>3</sub>, and then dried at 120 °C in a vacuum. As illustrated in Fig. 6b, 1–3 can be reused in at least five runs with a slight catalytic activity loss. PXRD patterns of 1–3 after catalysis showed good crystallinity, indicating that the structures have remained stable (Fig. S15–S17†). Additionally, the metal leaching experiments of 1–3 after catalysis were measured by ICP-OES. Almost no Mn<sup>2+</sup> can be detected, demonstrating that there is no obvious metal leaching in catalysis (0.11 mg L<sup>-1</sup>, 0.08 mg L<sup>-1</sup>, and 0.10 mg L<sup>-1</sup> for 1–3, respectively).

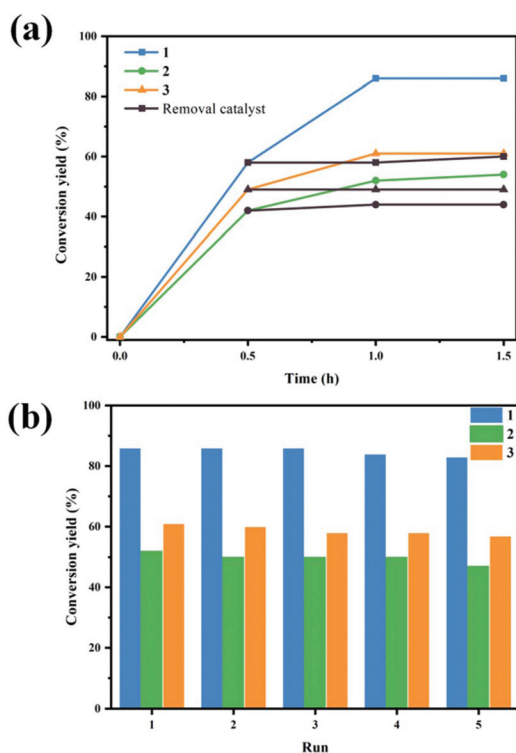


Fig. 6 (a) Effect of time on the yields. (b) The recycling catalytic studies of 1–3.

## Conclusions

In summary, using a low dimensional Mn(II) coordination polymer **1** as the precursor, three Mn(II) MOFs **2–4** have been synthesized by crystal transformation using three external stimuli. By adding 2,2'-bpy as the additional ligand and H<sub>2</sub>bqdc as the structural-directing agent, **1** can be transformed into **2** and **3**, respectively, with similar 3D topological networks, and by increasing the reaction temperature, **1** can be transformed into **4**. Moreover, **3** can also be transformed into **2** by adding 2,2'-bpy instead of coordinated water molecules and **3** can be transformed into **4** by prolonging the reaction time. Additionally, owing to different structures and catalytic active sites, **1** and **3** exhibit good catalytic activity, whereas **2** displays weak catalytic activity in cyanosilylation reactions. These results demonstrated that a crystal transformation strategy based on a low-dimensional precursor could effectively induce the construction of functional MOFs. Further work will focus on investigating the differences arising upon replacing the H<sub>3</sub>L ligand with other multi-carboxylate ligands toward the synthesis of new low-dimensional metal-organic precursors and their crystal transformation.

## Author contributions

The manuscript was written through contributions of all the authors. All authors approved the final version of the manuscript.

## Conflicts of interest

There are no conflicts to declare.

## Acknowledgements

The authors gratefully acknowledge financial support through the National Natural Science Foundation of China (No. 52075218 and 51775232) and the Science and Technology Development Plan Project of Jilin Province (No. 20190201155JC and 20190201278JC).

## Notes and references

- W. Xu, B. Tu, Q. Liu, Y. Shu, C.-C. Liang, C. S. Diercks, O. M. Yaghi, Y.-B. Zhang, H. Deng and Q. Li, *Nat. Rev. Mater.*, 2020, **5**, 764.
- A. Kirchon, L. Feng, H. F. Drake, E. A. Joseph and H. C. Zhou, *Chem. Soc. Rev.*, 2018, **47**, 8611.
- L. Feng, K. Y. Wang, G. S. Day, M. R. Ryder and H. C. Zhou, *Chem. Rev.*, 2020, **120**, 13087.
- J. R. Li, R. J. Kuppler and H. C. Zhou, *Chem. Soc. Rev.*, 2009, **38**, 1477.
- E. A. Dolgoplova, A. M. Rice, C. R. Martin and N. B. Shustova, Photochemistry and photophysics of MOFs: steps towards MOF-based sensing enhancements, *Chem. Soc. Rev.*, 2018, **47**, 4710.
- K. Lu, T. Aung, N. Guo, R. Weichselbaum and W. Lin, *Adv. Mater.*, 2018, **30**, e1707634.
- R. Li, W. Zhang and K. Zhou, *Adv. Mater.*, 2018, **30**, e1705512.
- A. Dhakshinamoorthy, Z. Li and H. Garcia, *Chem. Soc. Rev.*, 2018, **47**, 8134.
- J. Zhou and B. Wang, *Chem. Soc. Rev.*, 2017, **46**, 6927.
- T. Simon-Yarza, A. Mielcarek, P. Couvreur and C. Serre, *Adv. Mater.*, 2018, **30**, e1707365.
- W. Lu, Z. Wei, Z.-Y. Gu, T.-F. Liu, J. Park, J. Park, J. Tian, M. Zhang, Q. Zhang, T. Gentle III, M. Bosch and H.-C. Zhou, *Chem. Soc. Rev.*, 2014, **43**, 5561–5593.
- Y. Jiang, Z. Lu, P. Wang, J. Xu, L. Wang and Y. Fan, *Microporous Mesoporous Mater.*, 2020, **308**, 110568.
- N. Stock and S. Biswas, *Chem. Rev.*, 2012, **112**, 933.
- S. Li, M. Wu, Y. Kang, H. W. Zheng, X. J. Zheng, D. C. Fang and L. P. Jin, *Inorg. Chem.*, 2019, **58**, 4626.
- M. Nihei, L. Han, H. Oshio and J. Am, *Chem. Soc.*, 2007, **129**, 5312.
- W.-W. He, S.-L. Li and Y.-Q. Lan, *Inorg. Chem. Front.*, 2018, **5**, 279.
- A. Chaudhary, A. Mohammad and S. M. Mobin, *Cryst. Growth Des.*, 2017, **17**, 2893.
- R. A. Agarwal, S. Mukherjee, E. C. Sañudo, S. K. Ghosh and P. K. Bharadwaj, *Cryst. Growth Des.*, 2014, **14**, 5585.
- L. Zhong, J. Ding, J. Qian and M. Hong, *Coord. Chem. Rev.*, 2021, **434**, 213804.

- 20 S. Yuan, J. S. Qin, H. Q. Xu, J. Su, D. Rossi, Y. Chen, L. Zhang, C. Lollar, Q. Wang, H. L. Jiang, D. H. Son, H. Xu, Z. Huang, X. Zou and H. C. Zhou, *ACS Cent. Sci.*, 2018, **4**, 105.
- 21 Y. Keum, S. Park, Y. P. Chen and J. Park, *Angew. Chem., Int. Ed.*, 2018, **57**, 14852.
- 22 L. X. Shi, W. F. Zhao, X. Xu, J. Tang and C. D. Wu, *Inorg. Chem.*, 2011, **50**, 12387.
- 23 Y. Jiang, J. Xu, Z. Zhu, C. Jiang, L. Ma, H. Wang, L. Wang and Y. Fan, *Inorg. Chim. Acta*, 2020, **510**, 119735.
- 24 J. Chai, P. Zhang, X. Shi, J. Sun, L. Wang and Y. Fan, *CrystEngComm*, 2019, **21**, 5440.
- 25 Y. Zhang, C. Huang and L. Mi, *Dalton Trans.*, 2020, **49**, 14723.
- 26 Y. Jiang, J. Sun, X. Yang, J. Shen, Y. Fu, Y. Fan, J. Xu and L. Wang, *Inorg. Chem.*, 2021, **60**, 2087.
- 27 J.-Z. Gu, S.-M. Wan, M. V. Kirillova and A. M. Kirillov, *Inorg. Chem. Front.*, 2021, **8**, 1229.
- 28 C. Feng, C.-P. Lv, H. Zhao, Z.-Q. Li, W.-N. Xie, L. N. Sun and Y. Wang, *Cryst. Growth Des.*, 2020, **20**, 5682.
- 29 S. Dawood, A. Dorris, K. Davis, N. I. Hammer and H. Rathnayake, *J. Phys. Chem. C*, 2020, **125**, 792.
- 30 A. Halder and D. Ghoshal, *CrystEngComm*, 2018, **20**, 1322.
- 31 J. Liu, Z. Wang, R. Bi, F. Mao, K. Wang, H. Wu and X. Wang, *Inorg. Chem. Front.*, 2020, **7**, 718.
- 32 Y. Li, D. Ma, C. Chen, M. Chen, Z. Li, Y. Wu, S. Zhu, G. Peng and J. Solid, *State Chem.*, 2019, **269**, 257.
- 33 H. Tabe, M. Matsushima, R. Tanaka and Y. Yamada, *Dalton Trans.*, 2019, **48**, 17063.
- 34 U. Kokcam-Demir, A. Goldman, L. Esrafil, M. Gharib, A. Morsali, O. Weingart and C. Janiak, *Chem. Soc. Rev.*, 2020, **49**, 2751.
- 35 W. Li, L. Sun, L. Xie, X. Deng, N. Guan and L. Li, *Chin. J. Catal.*, 2019, **40**, 1255.
- 36 L. Zhai, Y. Niu, X. Chen, Z. Dong, Y. Gao, Y. Zhang, B. Li and L. Fan, *Inorg. Chem. Commun.*, 2020, **119**, 108121.
- 37 J.-J. Du, X. Zhang, X.-P. Zhou and D. Li, *Inorg. Chem. Front.*, 2018, **5**, 2772.
- 38 S. Yuan, L. Feng, K. Wang, J. Pang, M. Bosch, C. Lollar, Y. Sun, J. Qin, X. Yang, P. Zhang, Q. Wang, L. Zou, Y. Zhang, L. Zhang, Y. Fang, J. Li and H. C. Zhou, *Adv. Mater.*, 2018, **30**, e1704303.
- 39 A. Tăbăcaru, C. Pettinari and S. Galli, *Coord. Chem. Rev.*, 2018, **372**, 1.
- 40 X.-M. Kang, M.-H. Tang, G.-L. Yang and B. Zhao, *Coord. Chem. Rev.*, 2020, **422**, 213424.